Acta Crystallographica Section B
Structural Science
ISSN 0108-7681

Structure and conformational analysis of a bidentate pro-ligand, $C_{21}H_{34}N_2S_2$, from powder synchrotron diffraction data and solid-state DFTB calculations

Edward E. Ávila,[a] Asiloé J. Mora,[a]* Gerzon E. Delgado,[a] Ricardo R. Contreras,[b] Luis Rincón,[c] Andrew N. Fitch[d] and Michela Brunelli[d]‡

[a]Laboratorio de Cristalografía, Departamento de Química, Facultad de Ciencias, Universidad de Los Andes 5101, Venezuela, [b]Laboratorio de Organometálicos, Departamento de Química, Facultad de Ciencias, Universidad de Los Andes 5101, Venezuela, [c]Grupo de Procesos Dinámicos en Química, Departamento de Química, Facultad de Ciencias, Universidad de Los Andes 5101, Venezuela, and [d]European Synchrotron Radiation Facility, BP 220, F-38043 Grenoble CEDEX, France

‡ Current address: ILL Institut Laue–Langevin, BP 156, 38042 Grenoble CEDEX 9, France.

Correspondence e-mail: asiloe@ula.ve

Received 9 March 2009
Accepted 10 July 2009

The molecular and crystalline structure of ethyl 1′,2′,3′,4′,4a′,5′,6′,7′-octahydrodispiro[cyclohexane-1,2′-quinazoline-4′,1″-cyclohexane]-8′-carbodithioate (I) was solved and refined from powder synchrotron X-ray diffraction data. The initial model for the structural solution in direct space using the simulated annealing algorithm implemented in *DASH* [David *et al.* (2006). *J. Appl. Cryst.* **39**, 910–915] was obtained performing a conformational study on the fused six-membered rings of the octahydroquinazoline system and the two spiran cyclohexane rings of (I). The best model was chosen using experimental evidence from ^{1}H and ^{13}C NMR [Contreras *et al.* (2001). *J. Heterocycl. Chem.* **38**, 1223–1225] in combination with semi-empirical AM1 calculations. In the refined structure the two spiran rings have the chair conformation, while both of the fused rings in the octahydroquinazoline system have half-chair conformations compared with in-vacuum density-functional theory (DFT) B3LYP/6-311G*, DFTB (density-functional tight-binding) theoretical calculations in the solid state and other related structures from X-ray diffraction data. Compound (I) presents weak intramolecular hydrogen bonds of the type N—H···S and C—H···S, which produce delocalization of the electron density in the generated rings described by graph symbols $S(6)$ and $S(5)$. Packing of the molecules is dominated by van der Waals interactions.

1. Introduction

Metal centers of Cu^{II} in plastocyanin or azurin (Roat-Malone, 2002), Ni^{II} in nickel hydrogenase (Kain & Schwederski, 1994) and Zn^{II} in the so-called 'zinc finger' proteins involved in the activation and regulation of the DNA transcription (Auld, 2001) have pseudo-tetrahedral coordination with the metal atom surrounded by ligands containing two N atoms and two S atoms as donor groups. Recently, a series of bidentate nitrogen–sulfur pro-ligands of the type $[NS]^{1-}$ were designed and synthesized with the purpose of introducing structural modifications that favor site distortions which approach the entatic state characteristic of the metalloprotein systems mentioned above (Contreras *et al.*, 2001, 2005, 2006). Some of these new pro-ligands were obtained as powders (Avila *et al.*, 2008). Here we report the molecular and crystalline structure of ethyl 1′,2′,3′,4′,4a′,5′,6′,7′-octahydrodispiro[cyclohexane-1,2′-quinazoline-4′,1″-cyclohexane]-8′-carbodithioate (I) solved and refined from synchrotron X-ray powder diffraction data.

Table 1
*AM*1 qualitative enthalpies of formation for the different conformers of (I), and the value of $\chi^2_{Profile}$ (χ^2_{Pawley} = 8.660) of the best solution for each conformer obtained with the direct space simulated annealing program *DASH*.

Initial model molecular for (I)					*AM*1	SA
No.	*A*	*B*	*C*	*D*	ΔH_f (kJ mol^{-1})	$\chi^2_{Profile}$
1	Half-chair	Half-chair	*syn*	*syn*	−44.271	243
2	Half-chair	Half-chair	*syn*	*anti*	−69.723	212
3	Half-chair	Half-chair	*anti*	*anti*	−70.594	40
4	Half-chair	Half-chair	*anti*	*syn*	−43.463	140
5	Half-chair	Boat	*syn*	*syn*	−36.370	234
6	Half-chair	Boat	*syn*	*anti*	−71.243	251
7	Half-chair	Boat	*anti*	*anti*	−63.221	110
8	Half-chair	Boat	*anti*	*syn*	−35.739	162

2. Experimental

2.1. General information

The UV–vis spectrum in a CH_2Cl_2 solution of (I) was recorded on a Shimadzu UV–vis UVmini-1240 spectrophotometer. The FTIR spectrum (5000–400 cm^{-1}) was taken in KBr pellets on a Fourier transform PE 1725X spectrophotometer. Room-temperature ^{1}H and ^{13}C NMR spectra in $CDCl_3$ solutions were recorded on a Bruker Avance DRX 400 MHz spectrometer. The mass spectrum was obtained using a Hewlett–Packard System 5988A GC-MS spectrometer using electronic impact ionization.

2.2. Synthesis of (I)

Carboxydithio dispirotetracyclohexane acid (6.8 g, 0.019 mol) synthesized as described in Contreras *et al.* (2001) was placed in a beaker containing a 100 ml solution of NaOH 2N, and allowed to stir for 24 h to obtain a suspension. The suspension was placed in a thermostatic bath between 263 and 268 K. Diethylsulfate (5.8 ml, 0.044 mol) was added dropwise, and the mixture stirred for 2 h. A yellow solid was collected by suction. Rectangular microcrystals were obtained by slow evaporation of the recrystallization solvent dioxane, giving a 40% overall yield. Melting point: 350.8–351.4 K. The diagram shows labeling of the various rings in the molecular structure of (I). Mass spectroscopy (MS) data using electronic ionization showed P+, *m*/*z* (I %): $C_{21}H_{34}N_2S_2$, 378.2 (12%). NMR data ($CDCl_3$, 400 MHz) (δ, p.p.m.): δ_H 14.87 (N—H, s, 1H); 3.19 (m, 2H); 2.90 (dd, 1H, J_1 = 14.8, J_2 = 4.3); 2.45 (td, 1H, J_1 = 14.6 and J_2 = 5.4); 2.33 (t, 1H, J = 7.4); 2,16 (dd, 1H, J_1 = 11.9 y J_2 = 5.7); 1.91–1.09 (m, 26 H); δ C 196.1 (—C═S), 161.4 (N—C═C—), 113.6 (N—C═C—), 67.9, 53.2, 48.1, 41.9, 41.5, 40.2, 37.8, 28.7, 28.2, 27.4, 26.5, 25.7, 24.5, 22.4, 21.9, 21.5, 20.6, 12.95. UV–vis data (CH_2Cl_2) [λ (nm), ε (M^{-1} cm^{-1})]: 240.6 (5519), 319.7 (10 139), 401.1 (26 147). FTIR data (KBr pellet) [λ, cm^{-1}, s = strong, m = medium, w = weak, br = broad]: ν(N—H_{bridge}), 3449 m, br; ν(N—H_{free}), 3282 m; ν(C═C) + ν_a(C═N), 1588 s; ν_s(C═C), 1477 m; ν_s(C═N) + ν_a(C═S), 1365 m; ν_a(S—CH_2—), 1273 m; ρ-CH_2, 946 w; ν_a(CSS—), 911 w; ν_s(CSS—), 778 w.

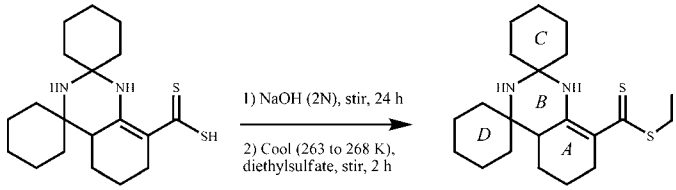

(I)

2.3. X-ray crystallography

X-ray powder diffraction data were collected with the high-resolution powder X-ray diffractometer on beamline ID31 at ESRF (Fitch, 2004), using X-rays with a wavelength of 0.80098 (5) Å. In order to obtain a homogeneous powder, a small amount of (I) was lightly ground with a pestle in an agate mortar and introduced into a 1.0 mm diameter borosilicate glass capillary, mounted on the axis of the diffractometer and spun during measurements. Data were collected and normalized against monitor counts and detector efficiencies and rebinned into steps of 2θ = 0.003°.

The auto-indexing program *DICVOL* (Boultif & Loüer, 2004) indexed the diffraction pattern in a monoclinic cell, with cell parameters a = 21.7356 (4), b = 10.0565 (2), c = 9.4511 (2) Å, and β = 99.9602 (8)° (refined) and figures of merit M_{20} = 65.5 (de Wolff, 1968) and F_{20} = 385.6 (0.0016, 33; Smith & Snyder, 1979). Systematic absences unequivocally assigned the space group as $P2_1/n$ (No. 14).

In order to solve the structure, the simulated annealing method implemented in the program *DASH*3.0 (David *et al.*, 2006) was chosen. However, a key step in any structural solution by this method is to access a molecular model whose conformation matches as closely as possible that of the molecule whose crystal structure is to be found. In the case of this study, this step required a thorough analysis of all the conformers arising from the different arrangements adopted by the spiro cyclohexane rings (*C* and *D*) and the unsaturated fused cyclohexene ring (*B*). Ring *A* was restricted to adopt a half-chair conformation as confirmed by the analysis of the uni- and bi-dimensional ^{1}H and ^{13}C NMR spectra (Contreras *et al.*, 2001). Table 1 contains the resulting eight models and the nomenclature used to distinguish them. To optimize the proposed structures, theoretical AM1 (Dewar *et al.*, 1995) calculations were run using the program *PC Spartan Plus* (Deppmeier *et al.*, 2002). Note that AM1 is in general an adequate theoretical tool for conformational analysis (Pop *et al.*, 2002; Munro & Camp, 2003: Munro & Mariah, 2004). In the models ring *B* adopts either the boat or half-chair conformations. On the other hand, *C* and *D* are spiro rings and therefore can only adopt the chair conformation as seen in 30 related spiro cyclohexane rings found in the Cambridge Structural Database (CSD; Allen, 2002). The combination of all these conformations gives rise to only two conformers. However, the spatial orientation of the *C* and *D* rings in relation to the octahydroquinazolidine system had to be taken into account and, hence, eight conformers have been considered (see Table 1). The description of the nomenclature used

Table 2
Experimental details.

Crystal data	
Chemical formula	$C_{21}H_{34}N_2S_2$
M_r	378.64
Crystal system, space group	Monoclinic, $P2_1/n$
Temperature (K)	298
a, b, c (Å)	21.7356 (4), 10.0565 (2), 9.4510 (2)
β (°)	99.9602 (8)
V (Å^3)	2034.72 (7)
Z	4
Radiation type	Synchrotron radiation
Wavelength of incident radiation (Å)	0.80098 (5)
μ (mm−1)	0.00
Specimen form, size (mm)	Cylinder (particle morphology: thin powder), 40.0 × 1.0 × 1.0
Specimen preparation temperature (K)	298
Data collection	
Diffractometer	Beamline ID31
Specimen mounting	Borosilicate glass capillary
Scan method	Step
Data-collection mode	Transmission
Absorption correction	None
2θ values (°)	$2\theta_{min}$ = 3.00, $2\theta_{max}$ = 50.00, $2\theta_{step}$ = 0.003
Refinement	
Refinement on	Intensity
R_p, R_{wp}, R_{exp}, R_{F^2}, χ^2	0.044, 0.054, 0.024, 0.1263, 5.29
Excluded region(s)	None
Profile function	Pseudo-Voigt
No. of parameters	127
No. of restraints	186
H-atom treatment	Constrained
$(\Delta/\sigma)_{max}$	0.05
Extinction method	None
Preferred orientation correction	Spherical harmonic

Computer programs used: *DASH* (David *et al.*, 2006), *GSAS* (Larson & Von Dreele, 2007), *EXPGUI* (Toby, 2001), *DIAMOND* 2.1e (Brandenburg, 2001), *GSAS2CIF* (Toby *et al.*, 2003), *PLATON* (Spek, 2009), *publCIF* (Westrip, 2009).

in Table 1 is as follows: the *syn–syn* notation corresponds to bonds C9—C10 and C12—C13 in ring *C*, C14—C15 and C17—C18 in ring *D* being perpendicular to bonds C1—N1 and C2—C8 of ring *B*. Likewise, the *anti–anti* notation corresponds to bonds C9—C10 and C12—C13 in ring *C*, C14—C15 and C17—C18 in ring *D* being parallel to bonds C1—N1 and C2—C8 of ring *B*, respectively. Crossover conformations also exist, *syn–anti* and *anti–syn*. All these conformations are shown in Fig. 1.

Once all the models were constructed, each one was introduced into *DASH* (David *et al.*, 2006) as a *z*-matrix, allowing the model to have six external and three internal degrees of freedom. Each of the runs took 5 h on a regular Pentium 4 Dual-Core PC desktop. The preliminary Pawley (1981) refinement routine of the program extracted 596 unique reflections in the 2θ range 3.005–30.355° from the powder diffraction data affording a figure of merit χ^2_{Pawley} = 8.660. The solution of the crystal structure was obtained after running the simulated annealing routine with a termination criterion of $\chi^2_{run} = 3\chi^2_{Pawley}$ in order to reduce the number of solutions. The conformer *anti–anti* with ring *A* adopting the half-chair conformation afforded the structural solution with a $\chi^2_{Profile}$ of 40, approximately 5 times χ^2_{Pawley} (see Table 1). The structure was refined with the Rietveld (1969) program *GSAS* (Larson & Von Dreele, 2007) using the graphical interface *EXPGUI* (Toby, 2001).

The H atoms were placed in calculated positions with restricted geometries using the HFIX command of the program *SHELXL* (Sheldrick, 2008). The peak shapes were modeled using the pseudo-Voigt peak shape function 4 (Thompson *et al.*, 1987), which included the axial divergence correction at low angle (Finger *et al.*, 1994) and the anisotropic line-shape broadening model (Stephens, 1999). Background was initially determined manually and then modeled using the Chebyshev polynomial function. Restraints were applied to bond distances (deviations ± 0.01 Å) and bond angles (deviations ± 1°) using average values derived with the program *MOGUL*1.1 (Bruno *et al.*, 2004) run on the CSD (Allen, 2002). Restraints involving H atoms were kept tight with deviations for bond distances and bond angles set at ± 0.005 Å and ± 1°.

The isotropic atomic displacement parameters were refined as one overall U_{iso} for the non-H atoms starting from a value of 0.03 Å^2. The isotropic displacement coefficients of each of the H atoms were refined as 1.3 times the value of the temperature factor of their riding non-H atom. The refinement was stable and convergence was readily achieved.

Finally, to inquire if the diffraction data contain systematic errors or if modeling of the peaks shapes and background was correct, a refinement without a model (Le Bail *et al.*, 1988) was conducted. The Le Bail refinement produced excellent agreement factors: R_p = 0.031, R_{wp} = 0.038, and χ^2 = 2.588, which do not differ greatly from the Rietveld agreement factors: (with background/without background) R_p/R'_p = 0.044/0.048, R_{wp}/R'_{wp} = 0.054/0.059, R_{exp} = 0.024, R_{F^2} = 0.1263 (1374 reflections) and χ^2 = 5.307; therefore, the problems described

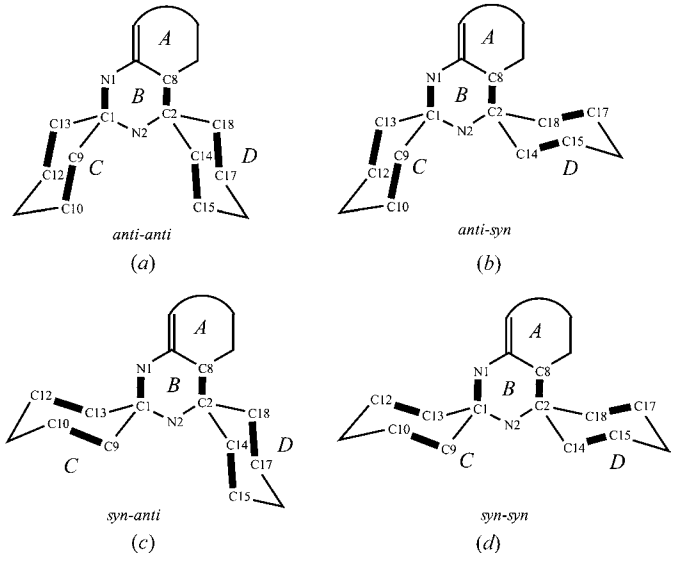

Figure 1
Schematic representation of the nomenclature used to describe the spatial disposition of rings *C* and *D* towards the octahydroquinazolidine system. The conformation of ring *A*, which can be half-chair or boat, is not shown. The configuration *anti-anti* with ring *A* as a half-chair led to the crystal structural solution with the lowest $\chi^2_{Profile}$.

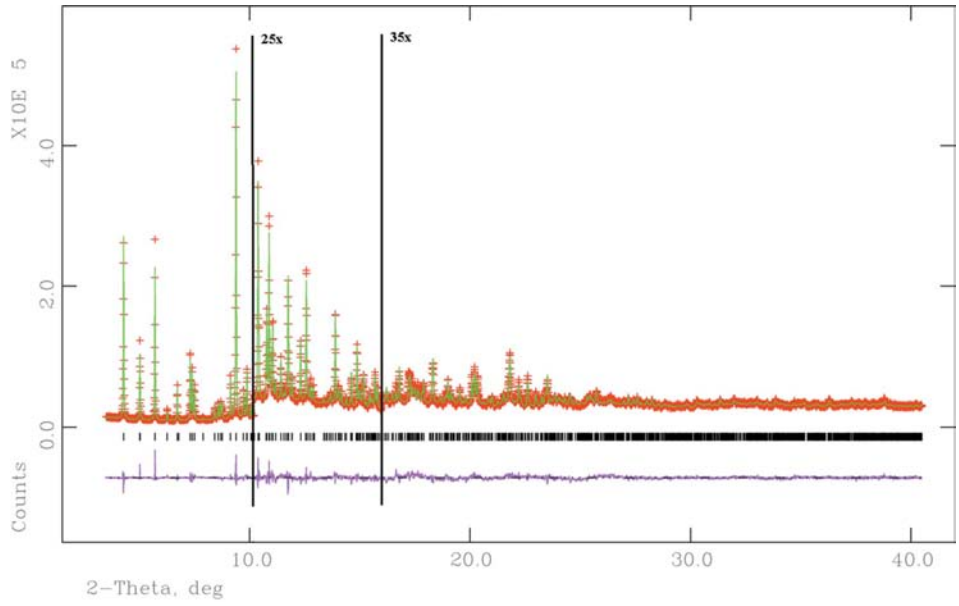

Figure 2
Final observed (points), calculated (lines) and difference profiles of the Rietveld plot for (I). The vertical scale of the 10.2 and 16.0° portions of the profiles has been multiplied by a factor of 25 and 35, respectively.

above were ruled out. Residuals in the last Fourier map were +0.37 and −0.47 e Å^{-3}.

Fig. 2 shows the final Rietveld plot, while Table 2 displays experimental details for the data collection, structural solution and the Rietveld refinement.[1]

2.4. Theoretical calculations

2.4.1. Solid-state DFTB calculations. The DFTB approximation (Porezag *et al.*, 1995; Elstner *et al.*, 1998) is a tool for the electronic structure simulation of systems with many atoms (up to 1000), particularly in periodic three-dimensional systems such as crystals. To determine the total energy and the inter-atomic forces for a given set of atomic positions, the calculations are based on the approximation of two-center pairs with a non-orthogonal basis set for the matrix elements of $\hat{H}^0$. Therefore, the generalized eigenvalues and eigenvectors problem is computed by the explicit evaluation of the elements of the matrix of the overlap integrals $S_{ij} = \langle\varphi_i|\varphi_j\rangle S_{ij}$ and Hamiltonians $H_{ij} = \langle\varphi_i|\hat{H}^0|\varphi_j\rangle$. The $|\varphi_j\rangle$ basis sets are eigenfunctions from density-functional theory/local density approximation (DFT/LDA) calculations of a single atom in a confined potential (Eschrig, 1988).

Self-consistent periodic DFTB calculations on (I) were performed using the *DFTB+* program (Elstner *et al.*, 1998, http://www.dftb-plus.info/) with the mio-0-1 set of parameters (http://www.dftb.org/). The following input parameters were used: DFT/LDA potentials (Porezag *et al.*, 1995), Broyden mixer in the self-consistent part and conjugate gradient relaxation iterative optimizations of the wavefunctions. The Monkhorst–Pack scheme (Monkhorst & Pack, 1976), using the supercell-folding routine contained in the program *DFTB+*. *A posteriori* dispersion corrections for the van der Waals interactions were applied (Elstner *et al.*, 2000, 2001).

Atomic-coordinate-only optimizations of (I) were performed in a supercell with *P*1 symmetry using as the initial geometry the experimental cell parameters and atomic positions obtained from the X-ray powder diffraction Rietveld refinement. The structure was evaluated and compared with the structure obtained from X-ray powder diffraction.

2.4.2. Density-functional calculations. DFT quantum chemical calculations were performed with Becke's three-parameter hybrid functional (Becke, 1993) and the correlation functional of Lee *et al.* (1988) using the 6-311G* basis set, B3LYP/6-311G*. All calculations were carried out using the *GAUSSIAN*03 (Revision B.02) suite of programs (Frisch *et al.*, 2003).

3. Results and discussion

3.1. Molecular conformation of (I)

Fig. 3 shows the molecular structure and the atom labeling of (I). The structure is basically built up from a rigid octahydroquinazolidine two-ring system (*A* and *B*); joined in positions 2 (C1) and 4 (C2) by two spiro cyclohexane rings (*C*

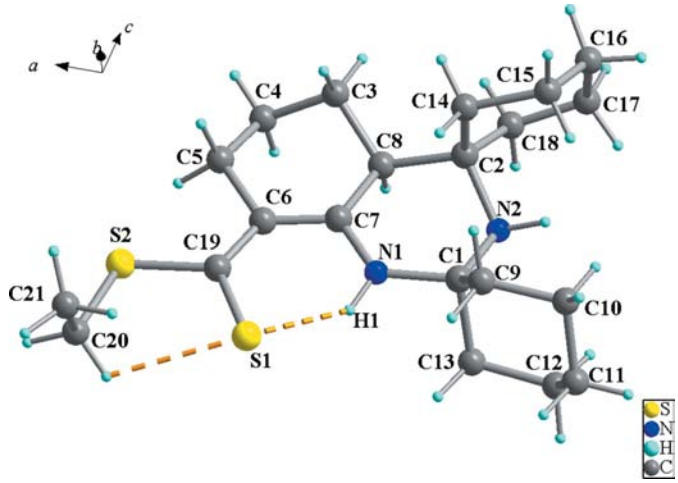

Figure 3
The asymmetric unit of (I) showing the atom-labeling scheme.

[1] Supplementary data for this paper are available from the IUCr electronic archives (Reference: ZB5006). Services for accessing these data are described at the back of the journal.

Table 3
Relevant bond distances (Å), bond angles (°) and torsion angles (°) for (I) from X-ray compared with solid-state DFTB and in-vacuum DFT calculations, and averages derived from related structures using *MOGUL*1.1.

	XRD	DFTB	DFT	MOGUL	Δ(XRD/DFTB)	Δ(XRD/DFT)	Δ(XRD/Mogul)	Δ(DFTB/DFT)	Δ(DFTB/Mogul)	Δ(DFT/Mogul)
S1—C19	1.717 (6)	1.701	1.697	1.66 (2)	0.016	0.020	0.057	0.004	0.041	0.037
S2—C19	1.721 (6)	1.788	1.803	1.74 (2)	−0.067	−0.082	−0.019	−0.014	0.048	0.063
S2—C20	1.787 (5)	1.838	1.829	1.81 (1)	−0.051	−0.042	−0.023	0.009	0.027	0.019
N1—C1	1.456 (6)	1.452	1.468	1.47 (1)	0.004	−0.012	−0.014	−0.016	−0.018	−0.002
N1—C7	1.330 (6)	1.338	1.337	1.34 (3)	−0.007	−0.007	−0.010	0.001	−0.003	−0.003
N2—C1	1.440 (5)	1.450	1.472	1.46 (2)	−0.010	−0.032	−0.020	−0.022	−0.010	0.012
N2—C2	1.459 (5)	1.462	1.484	1.48 (2)	−0.003	−0.025	−0.021	−0.022	−0.018	0.004
C2—C8	1.529 (6)	1.545	1.562	1.55 (1)	−0.016	−0.033	−0.021	−0.017	−0.005	0.012
C3—C4	1.502 (5)	1.507	1.522	1.53 (2)	−0.004	−0.020	−0.028	−0.016	−0.024	−0.008
C3—C8	1.520 (5)	1.522	1.522	1.53 (1)	−0.002	−0.002	−0.010	−0.001	−0.008	−0.008
C4—C5	1.489 (5)	1.515	1.525	1.52 (2)	−0.026	−0.036	−0.031	−0.009	−0.005	0.005
C5—C6	1.499 (5)	1.516	1.528	1.51 (1)	−0.017	−0.029	−0.006	−0.012	0.011	0.023
C6—C19	1.438 (7)	1.430	1.431	1.433 (7)	0.008	0.007	0.005	−0.001	−0.003	−0.002
C6—C7	1.416 (6)	1.420	1.409	1.35 (3)	−0.004	0.007	0.066	0.011	0.070	0.059
C7—C8	1.490 (6)	1.508	1.527	1.50 (1)	−0.018	−0.037	−0.010	−0.020	0.008	0.027
C20—C21	1.488 (4)	1.508	1.526	1.50 (5)	−0.021	−0.039	−0.034	−0.018	−0.013	0.005
C1—C9	1.533 (5)	1.535	1.556	1.529 (6)	−0.002	−0.023	0.004	−0.021	0.006	0.027
C1—C13	1.542 (5)	1.537	1.545	1.529 (6)	0.005	−0.003	0.013	−0.009	0.008	0.016
C19—S2—C20	104.7 (3)	106.47	105.83	104.1 (8)	−1.8	−1.1	0.6	0.6	2.4	1.7
C1—N1—C7	126.8 (4)	128.07	125.02	120 (4)	−1.3	1.8	6.8	3.1	8.1	5.0
C1—N2—C2	118.0 (4)	119.88	119.18	119 (3)	−1.9	−1.2	−1.0	0.7	0.9	0.2
N2—C1—C13	107.4 (3)	108.47	110.05	109 (1)	−1.1	−2.7	−1.6	−1.6	−0.5	1.1
N1—C1—C13	105.8 (4)	107.45	106.95	109 (1)	−1.7	−1.2	−3.2	0.5	−1.6	−2.1
N1—C1—N2	112.5 (3)	110.81	111.46	108 (2)	1.7	1.0	4.5	−0.7	2.8	3.5
N1—C1—C9	108.1 (4)	107.58	109.43	109 (1)	0.5	−1.3	−0.9	−1.9	−1.4	0.4
N2—C1—C9	114.1 (3)	113.94	110.51	109 (1)	0.2	3.6	5.1	3.4	4.9	1.5
N2—C2—C8	110.0 (3)	106.87	107.42	108 (1)	3.1	2.6	2.0	−0.6	−1.1	−0.6
N2—C2—C14	113.1 (3)	113.47	107.33	109 (1)	−0.4	5.8	4.1	6.1	4.5	−1.7
N2—C2—C18	102.4 (3)	106.51	111.62	109 (1)	−4.1	−9.2	−6.6	−5.1	−2.5	2.6
C4—C3—C8	105.6 (3)	108.52	109.95	111 (2)	−2.9	−4.4	−5.4	−1.4	−2.5	−1.1
C3—C4—C5	109.0 (3)	110.79	110.04	111 (3)	−1.8	−1.0	−2.0	0.8	−0.2	−1.0
C4—C5—C6	115.5 (3)	115.71	113.78	111 (2)	−0.2	1.7	4.5	1.9	4.7	2.8
C5—C6—C7	118.7 (4)	119.13	118.78	119 (3)	−0.1	0.2	0.0	0.4	0.1	−0.2
C5—C6—C19	114.7 (4)	115.89	118.01	118 (4)	−1.2	−3.3	−3.3	−2.1	−2.1	0.0
C7—C6—C19	126.3 (4)	124.96	123.82	–	1.3	2.5	–	1.1	–	–
N1—C7—C6	120.0 (4)	120.77	123.75	123 (2)	−0.8	−3.8	−3.0	−3.0	−2.2	0.8
C6—C7—C8	121.0 (4)	121.77	123.53	122.9 (7)	−0.8	−2.5	−1.9	−1.8	−1.1	0.6
N1—C7—C8	118.7 (4)	117.40	112.68	115.7 (5)	1.3	6.0	3.0	4.7	1.7	−3.0
C2—C8—C3	117.0 (3)	114.23	114.93	114 (2)	2.8	2.1	3.0	−0.7	0.2	0.9
C2—C8—C7	111.6 (3)	112.46	109.19	110 (2)	−0.9	2.4	1.6	3.3	2.5	−0.8
C3—C8—C7	111.1 (3)	110.50	113.96	108 (2)	0.6	−2.9	3.1	−3.5	2.5	7.0
S1—C19—C6	124.2 (4)	128.21	128.31	126.1 (7)	−4.0	−4.1	−1.9	−0.1	2.1	2.2
S2—C19—C6	116.5 (4)	114.05	112.82	113 (1)	2.5	3.7	3.5	1.2	1.0	−0.2
S1—C19—S2	119.0 (3)	117.74	118.87	122 (2)	1.3	0.1	−3.0	−1.1	−4.3	−3.1
S2—C20—C21	112.1 (3)	112.61	114.26	113.2 (2)	−0.5	−2.2	−1.1	−1.7	−0.6	1.1
C7—C6—C19—S1	14.9	8.2	−5.0	–	–	–	–	–	–	–
C20—S2—C19—S1	−1.0	−1.5	2.0	–	–	–	–	–	–	–
C20—S2—C19—C6	−174.8	−179.9	−177.5	–	–	–	–	–	–	–
C19—S2—C20—C21	91.3	83.3	85.7	–	–	–	–	–	–	–

and *D*), and in position 8 (C6) by a carbodithioate group. Table 3 shows selected bond distances, bond angles and torsion angles for (I) compared with those obtained from in-vacuum DFT B3LYP/6-311G* calculations, solid-state DFTB calculations, and with averages found with *MOGUL*1.1 (Bruno *et al.*, 2004) in searches based on related structural fragments run on the CSD (Allen, 2002). A detailed look at Table 3 shows the molecular structure of (I) obtained from powder X-ray diffraction data agrees very well with the solid-state DFTB calculations, with the average deviation for bond distances being 0.012 Å (largest deviations = +0.016 and −0.067 Å); for bond angles the average deviation is 0.37° (largest deviations = +3.1 and −4.0°). The correctness of the geometry of the refined molecule is also confirmed when it is compared with the *MOGUL*1.1 average distances and angles. For bond distances, the average deviation is 0.006 Å (largest deviations = +0.066 and −0.034) and for bond angles, the average deviation is 0.27° (largest deviations = +0.80 and −6.60°). When the Rietveld refined molecule is compared with the in-vacuum DFT optimized molecule, slightly larger deviations are observed, particularly associated with angles N2—C2—C18 and N2—C2—C14. These differences in angular values confirmed the slightly different orientation adopted by the spiran ring *D* in the in-vacuum molecule, which

Table 4
Intramolecular hydrogen bonds in (I).

D—H···A	H···A (Å)	D···A (Å)	D—H···A (°)
N1—H11···S1	2.04	2.900 (5)	147
C5—H52···S2	2.42	2.837 (5)	104
C20—H201···S1	2.46	3.016 (4)	115

inclines towards the octahydroquinazoline system most likely due to a repulsive electronic effect associated with the N2 lone pair.

Conformations of rings *A*, *B*, *C* and *D* were evaluated under the criteria described by Griffin *et al.* (1984). Rings *A* and *B* were confirmed to adopt the distorted half-chair conformation as shown by the C_s mirror plane passing through atoms C3 and C6, in ring *A*, and N1 and C2, in ring *B*, with values for ΔC_s = 14.0 (6) and 3.0 (5)°. The spiro rings *C* and *D* adopt chair conformations since they also display mirror planes passing through atoms C10 and C13 with ΔC_s = 2.1 (3)°, and C4 and C17 with ΔC_s = 2.9 (3)°, correspondingly; additionally both rings have C_2 binary axes passing through the midpoints of bonds C10—C11 and C1—C13 for ring *C* with ΔC_2 = 2.9 (3)°, C14—C15 and C17—C18 for ring *D* with ΔC_2 = 1.2 (4)°.

The mixed hybridization states of atoms C6, C7 (sp^2) and C3, C4, C5, C8 (sp^3) make ring *A* very asymmetric. Average bond distances are: Csp^2—Csp^2 = 1.416 (6) Å, Csp^2—Csp^3 = 1.49 (1) Å, Csp^3—Csp^3 = 1.50 (2) Å, which are in the range of the averages obtained from a search in the CSD (Allen, 2002) using *MOGUL*1.1 (Bruno *et al.*, 2004): 1.39 (6), 1.50 (3) and 1.52 (3) Å. On the other hand, the average bond angles for ring *A* are: Csp^2—Csp^2—Csp^3 = 119.9 (8), Csp^2—Csp^3—Csp^3 = 113.3 (7), Csp^3—Csp^3—Csp^3 = 107.3 (6)°, which agree well with average bond angles in related structures obtained with *MOGUL* 1.1: 123 (4), 122 (4) and 111 (3)°.

For similar reasons ring *B* is asymmetric. Atoms C7 and N1 are sp^2, while atoms C1, N2, C2 and C8 are sp^3. The average bond distances are: Nsp^2—Csp^2 = 1.330 (6) Å, Nsp^3—Csp^3 = 1.450 (1), Nsp^2—Csp^3 = 1.456 (6) and Csp^3—Csp^3 = 1.529 (6) Å. The average bond angles are: Csp^2—Nsp^2—Csp^2 = 126.8 (4), Nsp^2—Csp^3—Csp^3 = 106.9 (8), Nsp^3—Csp^3—Csp^3 = 109 (2)°, which within the s. u. match those found in related structures using *MOGUL*1.1: 123 (4), 111 (3) and 111 (3)°.

The S1—C19 bond distance, of the thione group, and the two S—C bond distances of the thioester group, S2—C19 and S2—C20, are 1.717 (6), 1.721 (6) and 1.787 (5) Å. These values agree with those found in related carbodithioates found in the CSD: *N*,*N*′-bis(2-amino-1-cyclopentencarbodithioate) (MEAMPT10; Sarkar & Gupta, 1981), *N*,*N*′-(3,6-diazaoctane)-bis(2-amino-1-cyclopentencarbodithioate) methyl (BEJYUK10; Sarkar & Gupta, 1982*a*), *N*,*N*′-diethylamino-bis(2-amino-1-cyclopentencarbodithioate) methyl (BIBSUA; Sarkar & Gupta, 1982*b*), (*R*)-bis(*N*-phenylethyl-2-amino-1-cyclopentenmercaptomethyl disulfur (GUDSUT; Cea-Olivares *et al.*, 1999), 2,2′-(propan-1,3-diyldiimino)bis(cyclopent-1-en-1-carbodithioate) dibenzyl (SAZJOT; Contreras *et al.*, 2006) and cycloheptanspiro-3′(4′*H*)-6′,7′,8′,9′-tetrahydrocyclohexa[b][1,4]thiazole-2′(5′*H*)-thione (Avila *et al.*, 2008). Additionally, the carbodithioate group is almost planar as illustrated by the torsion angle C7—C6—C19—S1 being close to 14.9°. On the other hand, the torsion angle C19—S2—C20—C21 is 91.3 (5)°, which indicates that the ethyl substituent is perpendicular to the plane described by S1, C19, S2, C7 and C6.

3.2. Intramolecular hydrogen bonding in (I)

Compound (I) displays intramolecular hydrogen bonds of the type N—H···S and C—H···S, whose geometric descriptions are given in Table 4. The formation of such hydrogen bonds (see Fig. 4) was previously reported by Contreras *et al.* (2006), giving rise to cycles of six and five members and described by the graph symbols *S*(6) and *S*(5) (Etter, 1990). These cycles stabilize the hydrogen-bond formation due to electronic charge-density delocalization amongst the atoms S1, C19, C6, C7, N1, H1 and S1, C19, S2. These findings are consistent with the reported FTIR spectra of (I) (Contreras *et al.*, 2004), which display two types of asymmetric stretching bands, υN—H:

(i) a weak and broad band at 3449 cm^{-1} assigned to the secondary amine participating in the N1—H1···S1 hydrogen bond;

(ii) a narrow band with intermediate intensity at 3282 cm^{-1} assigned to the secondary amine N2—H2.

There are essentially two factors which are responsible for the formation of these intramolecular hydrogen bonds. Firstly, the planarity of the *S*(6) ring system formed by the atoms S1,C19, C1, C2, N1 and H1 with deviations from planarity being less than ± 0.2 Å. Secondly, the relocation of electron charge density over the *S*(6) ring as shown by the Mulliken charges over the atoms derived from the theoretical DFTB calculations, which are shown in Fig. 4; atoms S1, N1 and C6 are negatively charged, while H1 and C7 are positively charged. S1 becomes an acceptor of H atoms and hence favoring the S1···H1 hydrogen bond. The *S*(5) ring is less planar and the delocalized electron density is only significant through S1—C19—S2. To explore the possibility of the formation of the

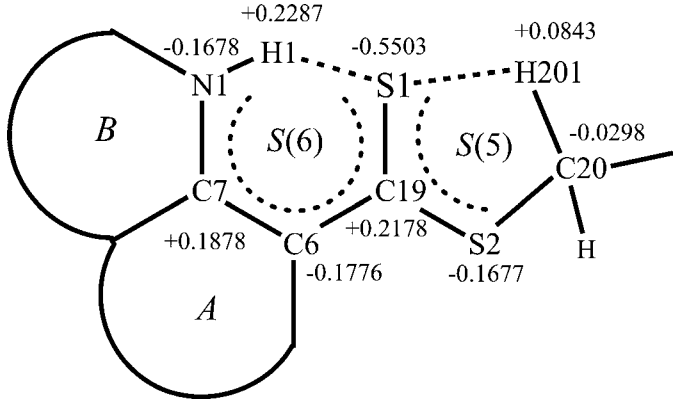

Figure 4
Diagram showing the relocation of electron charge density over ring *S*(6) and *S*(5) that favor the formation of intramolecular hydrogen bonds in (I). Mulliken charges over the atoms were calculated from DFTB.

C—H···S hydrogen bond which closes the *S*(5) ring (see Fig. 4), density-functional calculations were performed using a B3LYP/6-311G* level using the *GAUSSIAN*03 program (Frisch *et al.*, 2003) on an isolated molecule of (I). We varied stepwise the C19—S2—C20—H201 torsion angle between 0 and 360°, in steps of 45°, optimizing at each step all the other geometrical parameters. There are two energy barriers, one between the minima of H201 and H202, and the other through the methyl group. The first energy barrier is of 0.42 kJ mol^{-1}, while the other is of 2.51 kJ mol^{-1}. From these values we can conclude that in vacuum there is free rotation of the methyl group around the S2—C20 bond; therefore, the electrostatic interaction between H201 and S2, essential for the hydrogen-bond formation, is negligible, which we expect will be the case in the crystal. However, in the crystal the frozen orientation of these groups has geometrical distances and angles which comply with those of a hydrogen bond, and correspond to the minimum energy of the in-vacuum DFT and solid-state DFTB calculations. Previously, in articles (Contreras *et al.*, 2006; Hou *et al.*, 2008; Tamasi *et al.*, 2009) involving N,S ligands these types of weak interaction have been acknowledged as hydrogen bonds, without any theoretical analysis.

3.3. Crystal packing

The crystal packing of (I) is dominated entirely by van der Waals interactions, in which corrugated layers of molecules alternatively oriented in the opposite direction along [100] pack along [010]. Fig. 5 shows how the concavity of molecules from successive layers complements each other to make an efficient packing with 68.1% of occupied space (Spek, 2009). Structural overlay of the crystal packing from powder X-ray data and from the DFTB solid-state theoretical calculations showed excellent agreement, with atom position r.m.s. being less than 0.060 Å.

4. Conclusions

From synchrotron powder diffraction data, the molecular and crystal structure of ethyl 1′,2′,3′,4′,4a′,5′,6′,7′-octahydrodispiro[cyclohexane-1,2′-quinazoline-4′,1″-cyclohexane]-8′-carbodithioate (I) have been solved, which required a careful combination of AM1 calculations and spectroscopic evidence to construct conformational models that matched as closely as possible that of the unknown compound. The powerful simulated annealing minimization method was then used to test all of the models against the diffraction data until the best solution was obtained with the model having the *anti–anti* orientation of the two spiran rings, with the hexahydropyrimidine ring (*B*) in the half-chair conformation. Later, in-vacuum DFT B3LYP/6-311G* and DFTB theoretical calculations allowed us to confirm the experimental solution and also to discuss the electronic and geometrical structure. We expect this combination of theory and experiment will become standard and will support future works concerning structural reports of organic compounds.

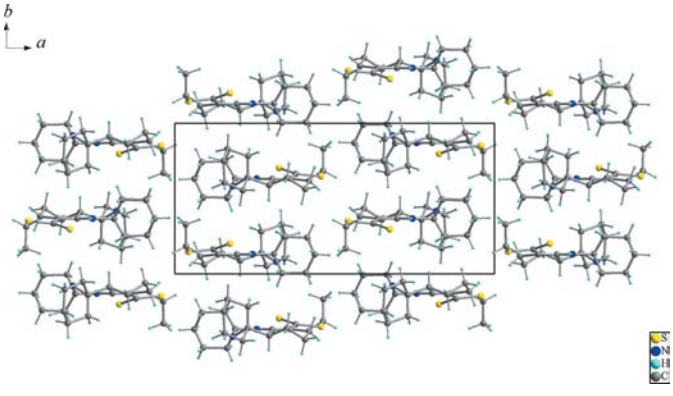

Figure 5
View of the packing of (I) molecules linked by van der Waals interactions along the (001) direction.

We thank beamline ID31, ESRF, for providing synchrotron radiation beam-time, the CDCHT-ULA (Subvention C-1511-07-08-B) and the FONACIT (Project LAB-97000821 and Subvention-200500703).

References

Allen, F. H. (2002). *Acta Cryst.* B**58**, 380–388.
Auld, D. S. (2001). *Handbook on Metalloproteins*, edited by I. Bertini, A. Sigel & H. Sigel, pp. 881–941. New York: Marcel Dekker, Inc.
Avila, E. E., Mora, A. J., Delgado, G. E., Contreras, R. R., Fitch, A. N. & Brunelli, M. (2008). *Acta Cryst.* B**64**, 217–222.
Becke, A. D. (1993). *J. Chem. Phys.* **98**, 5648–5652.
Boultif, A. & Louër, D. (2004). *J. Appl. Cryst.* **37**, 724–731.
Brandenburg, K. (2001). *DIAMOND*, Version 2.1e. Crystal Impact GbR, Bonn, Germany.
Bruno, I. J., Cole, J. C., Kessler, M., Luo, J., Motherwell, W. D. S., Purkis, L. H., Smith, B. R., Taylor, R., Cooper, R. I., Harris, S. E. & Open, A. G. (2004). *J. Chem. Inf. Comput. Sci.* **44**, 2133–2144.
Cea-Olivares, R., García-Montalvo, V., Hernández-Ortega, S., Rodríguez-Narvaéz, C., García, P. G., López-Cardoso, M., March, P., González, L., Elias, L., Figueredo, M. & Font, J. (1999). *Tetrahedron Asymm.* **10**, 3337–3340.
Contreras, R. R., Fontal, B., Bahsas, A., Reyes, M., Suárez, T. & Bellandi, F. (2001). *J. Heterocycl. Chem.* **38**, 1223–1225.
Contreras, R. R., Fontal, B., Bahsas, A., Reyes, M., Suárez, T., Bellandi, F., Nava, F. & Cancines, P. (2005). *Rev. Latinoam. Quím.* **33**, 7–11.
Contreras, R. R., Fontal, B., Bahsas, A., Suárez, T., Reyes, M., Bellandi, F., Nava, F. & Cancines, P. (2004). *Transition Met. Chem.* **29**, 51–55.
Contreras, R. R., Fontal, B., Romero, I., Atencio, R. & Briceño, A. (2006). *Acta Cryst.* E**62**, o205–o208.
David, W. I. F., Shankland, K., van de Streek, J., Pidcock, E., Motherwell, W. D. S. & Cole, J. C. (2006). *J. Appl. Cryst.* **39**, 910–915.
Deppmeier, B. J., Driessen, A. J., Hehre, W. J., Johnson, J. A., Klunzinger, P. E., Watanabe, M. & Yu, J. (2002). *PC Spartan Plus.* Wavefunction, Inc, Irvine, USA.
Dewar, M. J. S., Zoebisch, E. G., Healy, E. F. & Stewart, J. J. P. (1995). *J. Am. Chem. Soc.* **107**, 3902–3909.
Elstner, M., Porezag, D., Jungnickel, G., Elsner, J., Haugk, M., Frauenheim, T., Suhai, S. & Seifert, G. (1998). *Phys. Rev. B*, **58**, 7260–7268.
Elstner, M., Hobza, P., Frauenheim, T., Suhai, S. & Kaxiras, E. (2000). *Phys. Status Solidi B*, **217**, 357–376.

Elstner, M., Hobza, P., Frauenheim, T., Suhai, S. & Kaxiras, E. (2001). *J. Chem. Phys.* **114**, 5149–5155.
Eschrig, H. (1988). *Optimized LCAO Method and the Electronic Structure of Extended Systems.* Berlin: Akademie-Verlag.
Etter, M. C. (1990). *Acc. Chem. Res.* **23**, 120–126.
Finger, L. W., Cox, D. E. & Jephcoat, A. P. (1994). *J. Appl. Cryst.* **27**, 892–900.
Fitch, A. N. (2004). *J. Res. Natl. Inst. Stand. Technol.* **109**, 133–142.
Frisch, M. J. *et al.* (2003). *GAUSSIAN*03, Revision B.02. Gaussian Inc., Pittsburgh PA, USA.
Griffin, J. F., Duax, W. L. & Weeks, C. M. (1984). *Atlas of Steroid Structure*, Vol. 2, pp. 3–22. New York: IFI/Plenum Data Company, USA.
Hou, Y., Zhou, J., Liu, X., Yu, L. & Ni, Ch. (2008). *Transition Met. Chem.* **33**, 411–416.
Kain, W. & Schwederski, B. (1994). *Bioinorganic Chemistry: Inorganic Elements in the Chemistry of Life*, pp. 172–184. New York: Wiley, USA.
Larson, A. C. & Von Dreele, R. B. (2007). *GSAS.* Los Alamos National Laboratory, New Mexico, USA.
Le Bail, A., Duroy, H. & Fourquet, J. L. (1988). *Mater. Res. Bull.* **23**, 447–452.
Lee, C., Yang, W. & Parr, R. G. (1988). *Phys. Rev. B*, **45**, 13244–13249.
Monkhorst, H. J. & Pack, J. D. (1976). *Phys. Rev. B*, **13**, 5188–5192.
Munro, O. Q. & Mariah, L. (2004). *Acta Cryst.* B**60**, 598–608.
Munro, O. Q. & Camp, G. L. (2003). *Acta Cryst.* C**59**, o672–o675.
Pawley, G. S. (1981). *J. Appl. Cryst.* **14**, 357–361.
Pop, M. M., Goubitz, K., Borodi, G., Bogdan, M., De Ridder, D. J. A., Peschar, R. & Schenk, H. (2002). *Acta Cryst.* B**58**, 1036–1043.
Porezag, D., Frauenheim, T., Köhler, T., Seifert, G. & Kaschner, R. (1995). *Phys. Rev. B*, **51**, 12947–12957.
Rietveld, H. M. (1969). *J. Appl. Cryst.* **2**, 65–71.
Roat-Malone, R. M. (2002). *Bioinorganic Chemistry*, pp. 187–228. New Jersey: Wiley-Interscience.
Sarkar, P. B. & Gupta, S. P. S. (1981). *Cryst. Struct. Commun.* **10**, 1133–1137.
Sarkar, P. B. & Gupta, S. P. S. (1982*a*). *Cryst. Struct. Commun.* **11**, 433–438.
Sarkar, P. B. & Gupta, S. P. S. (1982*b*). *Cryst. Struct. Commun.* **11**, 439–444.
Sheldrick, G. M. (2008). *Acta Cryst.* A**64**, 112–122.
Smith, G. S. & Snyder, R. L. (1979). *J. Appl. Cryst.* **12**, 60–65.
Spek, A. L. (2009). *Acta Cryst.* D**65**, 148–155.
Stephens, P. W. (1999). *J. Appl. Cryst.* **32**, 281–289.
Tamasi, G., Defazio, S., Chiasserini, L., Sega, A. & Cini, R. (2009). *Inorg. Chim. Acta*, **362**, 1011–1021.
Toby, B. H. (2001). *J. Appl. Cryst.* **34**, 210–213.
Toby, B. H., Von Dreele, R. B. & Larson, A. C. (2003). *J. Appl. Cryst.* **36**, 1290–1294.
Thompson, P., Cox, D. E. & Hastings, J. B. (1987). *J. Appl. Cryst.* **20**, 79–83.
Westrip, S. P. (2009). *publCIF.* In preparation.
Wolff, P. M. de (1968). *J. Appl. Cryst.* **1**, 108–113.